Electronic Supporting Information

Materials

Tetramethylammonium hydroxide pentahydrate (TMAH•5H_2O), γ-glycidyl ether oxypropyl trimethoxysilane (KH560), methylbenzene, aminopropyltriethoxysilane (APTES), nano hexagonal boron nitride (h-BN), 4,4 '- diamino diphenyl ether (4,4' -ODA) and 4,4'-(4,4'-isopropyldiphenyloxy) phthalic anhydride (BPADA) were of analysis pure grade, purchased from Shanghai Maclean Biochemical Technology Co., China. Deionized water, sodium hydroxide aqueous solution (NaOH, 5 mol/L) and saturated saline were obtained in our lab. Isopropanol (IPA), Tetrahydrofuran (THF), N-methylpyrrolidone (NMP), anhydrous ethanol, anhydrous magnesium sulphate, N, N-Dimethylformamide (DMF), and absolute methanol were of Chemical pure grade, purchased from Chengdu Kelong Chemical Co., China. All chemicals are used directly without further purification or treatment.

Measurements

Structural characterization

^{1}H-NMR and ^{29}Si-NMR spectra were recorded on a Bruker ANANCE-400MHz NMR instrument. The infrared spectra were recorded using Fourier infrared spectroscopy (W QF-310) in the range of 400−4000 cm^{-1}. The crystal structure of the samples was characterized by an X-ray powder diffractometer (D8 DISCOVER A25, Germany) with CKα1 (λ = 1.54 Å) radiation.

The XPS spectra were obtained by X-ray photoelectron spectroscopy (XPS, Thermo Fisher Scientific, East Grinstead, UK) for the analysis of the valence, content, and electronic structure of each element on the surface of the material.

Scanning electron microscopy (SEM) images and energy dispersive X-ray (EDS) images were recorded by a Hitachi Regulus8100. High Resolution Transmission electron microscopy (HTEM, JEOL JEM-2100, 100 kV) was used to analyze the morphology and composition of the materials.

Thermal and mechanical performance testing

UV–vis spectra were performed on a UV-1800PC (Shanghai Mapada Co., Ltd.). The band gap of the composite film was determined by converting the transmittance data obtained from the test into the absorption coefficient.

$$(\alpha h\vartheta)^{n} = B(h\vartheta - Eg) \qquad \textit{(Eq. S1)}$$

Where α is the absorption coefficient, B is a constant, hv is the photon energy, h is the Planck constant, Eg represents the semiconductor bandgap width (bandgap); Direct bandgap: n=1/2; Indirect bandgap: n=2. Based on the calculated data, create a Tauc plot $(\alpha h\vartheta)^2 \sim h\vartheta$ and determine the band gap through linear extrapolation.

DSC was performed on a PerkinElmer DSC 8000 under nitrogen atmosphere with a heating rate of 10 °C min^{-1}. The profile analysis was carried out using VEGA 3 LMH scanning electron microscope from Tesken Trading Co., Ltd (Czech), and the accelerating voltage was 10KV.

Thermal gravimetric analysis (TGA) was performed by STA 449F3 (NETZSCH Co., Germany) thermal gravimetric analyzer. The test temperature range was 40 -800 ℃, and the heating rate was 10 ℃/min under argon atmosphere.

The tensile strength of the composites was tested by a CMT6303 electronic universal testing machine of New Sans Materials The variation of energy storage modulus and loss angle of the film material with temperature was tested using a Q800 Dynamic Mechanical Analyser (DMA). The temperature range was 80-260 °C at a fixed frequency of 1 Hz and a ramp rate of 5 °C/min.

Dielectric and energy storage performance testing

Dielectric constant (k) and dielectric loss tangent (tanδ) values of the samples were measured using a NoVo control Concept 50 broad frequency dielectric spectrometer with a frequency ranging from 1 Hz to 1 MHz. The prepolarisers were tested in a nitrogen atmosphere at a temperature increase rate of 5 °C/min.

A gold electrode with a thickness of 50 nm and a diameter of 10 mm was sputtered on the surface of the dielectric film to measure the dielectric constant and dielectric loss. The relative dielectric constant of the film is related to the electrode area as follows:

$$\varepsilon_r = \frac{Cd}{\varepsilon_0 A} \qquad (Eq.\ S2)$$

where ε_r is the relative permittivity of the material, A is the electrode area of the flat capacitor, d is the distance between the electrodes, which is the thickness of the film (about 15-20 μm), and ε_0 is the vacuum dielectric constant, which has a value of 8.85×10^{-12} F/m.

The temperature dependence of the depolarization current was obtained, namely the TSDC spectrum was obtained. The thickness of the specimen is about 20 microns and the surface is coated with a gold electrode with a thickness of 50 nm and a diameter

of 25 mm. Tested on a Poly K modified Sawyer-Tower circuit (oscilloscope graphical method) with a Trek 610C power amplifier. The temperature of the oil bath was 25 °C and 150 °C. The test frequency was 10 Hz, and the curves of the potential shift of the dielectric versus the strength of the electric field (D-E Loops) were measured. Boost rate 50 v/s, peak voltage of 10000 V for breakdown strength testing at 25 °C and 150 °C. Leakage current test with Keithley Electrostatic Meter Type 6517A at 25 and 150 °C and in the range of 10 to 200 MV/m. The test specimen preparation conditions for D-E loops and leakage currents are the same as for the dielectric spectrum test.

Experimental section

Synthesis of OG-POSS

POSS is used to modify various polymers to prepare organic and inorganic nano-hybrid composites due to its special structure. 200ml of IPA, 1.56g of TMAH-5H_2O , 14.05g of deionized water were added in a three-necked flask. An isopropanol solution of KH560 (30 ml of IPA, 60.38 g of KH560) was added dropwise (30 ml of IPA, 60.38 g of KH560) while stirring at room temperature, and stirred for 6 hours after the end of the drop. IPA was removed by distillation under reduced pressure, the product was dissolved in 200 ml of toluene, washed to neutrality with saturated brine, and dehydrated by adding sufficient anhydrous magnesium sulphate overnight.The product was filtered and added to a four-necked flask, and the weight of the product was noted as m_0. It is known that $m_{(hydrolysate)}$:$m_{(10\%\ TMAH\ aqueous\ solution)}$ =6.48:1, $m_{(TMAH\text{-}5H_2O)}$:$m_{(H_2O)}$ =1:4. m is known, and from the above ratios the mass of TMAH-5H_2O and H2O can be calculated, denoted as m_1 and m_2. The m_1 and m_2 were weighed and added to a four-necked flask, and the temperature was gradually increased to 108 °C for 6 hours. The cooled reaction solution was poured into a 1000 ml dispensing funnel and washed repeatedly to neutral and dehydrated. The product was evaporated under reduced pressure at 60 °C, collected and dried under vacuum at 70 °C in about 55.75% yield.

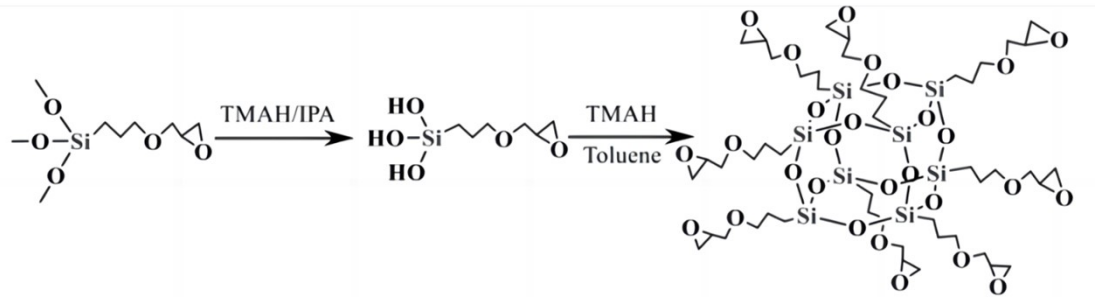

Fig. S1 The synthesis route of OG-POSS

Exfoliation of BNNS

h-BN powder (2 g) with an average diameter of 500 nm was added to 300 mL DMF and stirred vigorously for 1 h to ensure homogeneous dispersion, and sonicated in pulsed mode (70% amplitude) using an ultrasonic probe for 24 h. After the treatment it was allowed to stand to allow the unstripped h-BN to precipitate. The supernatant was collected by centrifugation at 10,000 rpm for 30 min (5000 rpm for 15 min) and the precipitate was collected from the wall of the centrifuge tube, washed with ethanol to remove the solvent and then dried in a vacuum oven at 60 °C for 24 h to obtain the white solid powder BNNS.

Hydroxylation and amination of BNNS

Firstly, the edge hydroxylation of h-BNNS was carried out. 0.5 g of h-BNNS was added into 500 mL NaOH (5 mol/L) with stirring and ultrasonication for 1 h to promote its homogeneous dispersion, and then it was poured into a three-necked flask equipped with a condenser tube and heated at 120 ℃ for 48 h. After cooling, it was filtered, and washed with ultrapure water to remove the NaOH, and then the pH value of it was detected with pH paper until it was neutral. After cooling, it was filtered and washed with ultrapure water to remove NaOH, and the pH value was tested with PH paper until it was neutral, and then it was dried in a vacuum oven at 80 °C for 12 h. The edge hydroxylation of BNNS was obtained, denoted as OH-BNNS.

APTES (3% of BNNS weight) was added to 100 mL of an aqueous ethanol solution, and the mixed solution was stirred at 60 °C for 30 min to complete the hydrolysis of APTES, followed by dispersing 2 g of OH- BNNS into the solution and stirring at 80 °C for 6 h. Filtration was carried out and washed with repeated washes with ethanol, and the mixture was dried at 80 °C for 24 h. The APTES-functionalized BNNS was obtained, denoted as NH_2-BNNS.

Preparation of 2D core-shell particles BNNS@POSS

OG-POSS was dissolved in anhydrous THF, mixed with amino-functionalized h-BNNS under ultrasonication and stirred at 60 °C for 4 h, ethanol washed and filtered, and dried in a vacuum oven at 80 °C for 24 h to obtain BNNS@POSS.

Calculation Section

DMA and TGA parameters

T_{HRI} is the heat resistance index temperature, which is obtained according to Eq. S3.

$$T_{HRI} = 0.49[T_5 + 0.6(T_{30} - T_5)] \quad \textit{(Eq. S3)}$$

Where T_5 and T_{30} is corresponding decomposition temperature of 5% and 30% weight loss, respectively.

The theoretical crosslink densities of samples in this work are all calculated by Eq. S4:

$$\rho = \acute{E} / 2(1 + \gamma)\, RT \qquad \textit{(Eq. S4)}$$

where γ is Poisson's ratio assumed as 0.5 for incompressible networks; R is gas constant, T is related to Tg +40 °C and É is the storage modulus of materials at Tg + 40 °C (obtained in dynamic thermomechanical analysis results).

Table S1 Thermal data for composite films

Sample	n	T_{d5} /°C	T_{d30} /°C	T_{HRI}	Y_C /%	T_g /°C	E /Mpa	ρ /(•10^{-3} mol/cm^3)
PEI	/	472.8	589.5	265.9	51.1	213.1	0.93	0. 22
BNNS@POSSn/PEI	2.5	484.8	595.9	270.1	53.0	217.4	1.06	0. 24
	5.0	492.83	589.2	269.8	56.2	233.3	1.18	0. 25
	7.5	501.6	600.9	274.9	56.7	228.2	1.08	0. 24
	10	502.3	598.4	274.3	57.3	231.7	1.03	0. 23

Molecular models construction

The molecular models of POSS and PEI were built in the Materials studio software package, and to simplify the computational scale, POSS was set as the original unit. Due to the insensitivity of the band gap of PEI to the chain length, the polymer was approximated by two repeating units with the degree of polymerization of PEI set to 2, and the structure was optimized by the DMol3 module.

DFT simulation

Density Functional Theory (DFT) simulations were performed in the DMol3 module of Materials Studio (2019, Accelrys Software Inc.) using the Gradient Approximation (GGA) with the Perdew-Burke-Ernzerhof (PBE) method to optimize the structure and to calculate the charge density, the LUMO/HOMO orbitals, and bandgap width properties.

Dielectric mechanism

Influence of dielectric constant in materials obeys Debye equation, as follows:

$$\frac{k-1}{k+2} = \frac{4\pi}{3} N(\alpha_e + \alpha_d + \frac{\mu^2}{3k_bT}) \qquad \textit{(Eq. S5)}$$

Where k is dielectric constant of the material, N, α_e, α_d, μ, k_b, and T are the density of the dipole, electron polarization, distortion polarization, orientation polarization related to the dipole moment, Boltzmann constant, and temperature, respectively.

TSDC calculation

The TSDC spectra of the samples were measured over a temperature range from -10 °C to 250 °C. The trap energy level can be calculated by processing the TSDC data through Eq. S6

$$A_{TSDC} = \frac{2.47 K_b T_p^2}{\Delta T} \quad (Eq.S6)$$

where ΔT is the temperature difference for the half-height peak, and T_p is the peak-current temperature. The trapped charge quantity can be calculated through Eq. S7:

$$Q = \left(\frac{60}{\vartheta}\right) \int_{T_1}^{T_0} I(T)dT \quad (Eq. S7)$$

where T_0 and T_1 is the starting and ending temperature of the peaks respectively, *I(T)* represent the TSDC curve, and υ is the heating rate after short circuit set to 3.0 K/min^{-1}.

Table S2. TSDC results and calculated trap parameters

Sample	Trap energy level-1 (eV)	Q_{TSDC} (nC)	Trap energy level-2 (eV)	Q_{TSDC} (nC)	Trap energy level-3 (eV)	Q_{TSDC} (nC)
Pure PEI	1.92	6.14	2.41	4.46	-	-
BNNS@POSS$_5$/PEI	1.88	36.4	2.48	13.6	2.96	12.5

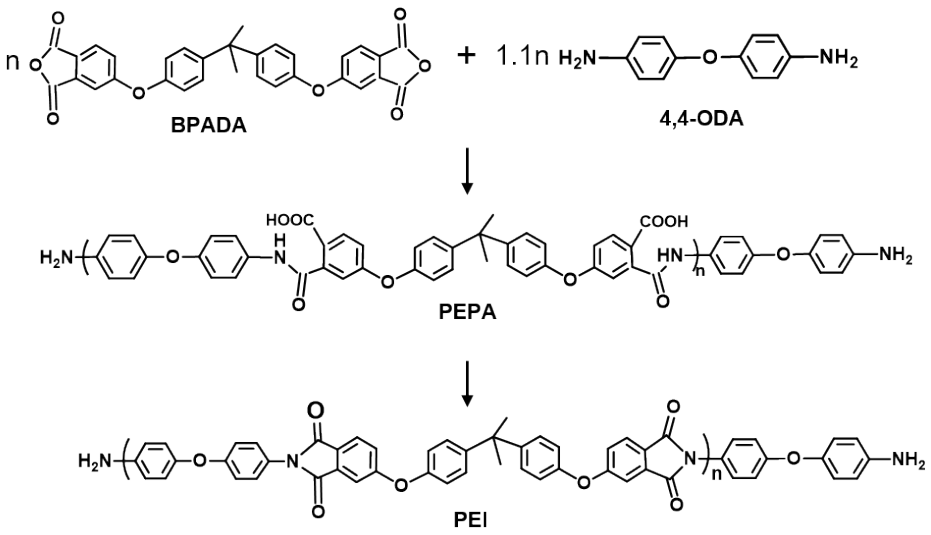

Fig. S2 Synthesis route of PEI

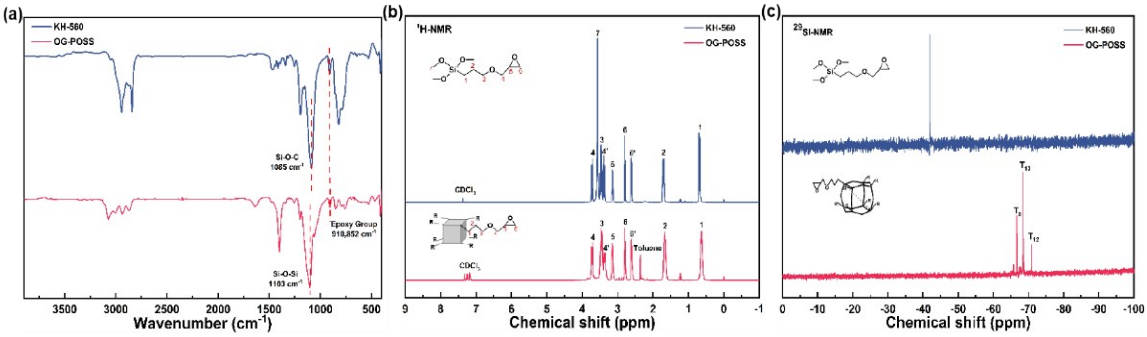

Fig. S3 The characterization of OG-POSS.

FT-IR(a), ^{1}H-NMR(b) and ^{29}Si-NMR(c) spectrums of KH-560 and OG-POSS.

The structures were characterized by FT-IR) and ^{1}H-NMR and ^{29}Si-NMR in Fig. S3. From the FT-IR, the vibration absorption peak of the Si-O-C and Si-O-Si vibration absorption peak at 1085 cm^{-1} and 1103 cm^{-1} respectively. And the epoxy group absorption peak at 910 cm^{-1}. Corresponding to this information is the ^{1}H-NMR of the OG-POSS, where the vibration at 2.61 ppm, 2.79 ppm, 3.15 ppm, 3.70 ppm, and 3.79 ppm can belong to the resonance signals of the proton on the glycidyl ether group (epoxy group). Meanwhile, three characteristic peaks of silicon at three different locations appeared at 66.74 ppm，68.51 ppm and 70.95 ppm, respectively. All the above analysis shows the successful synthesis of OG-POSS.

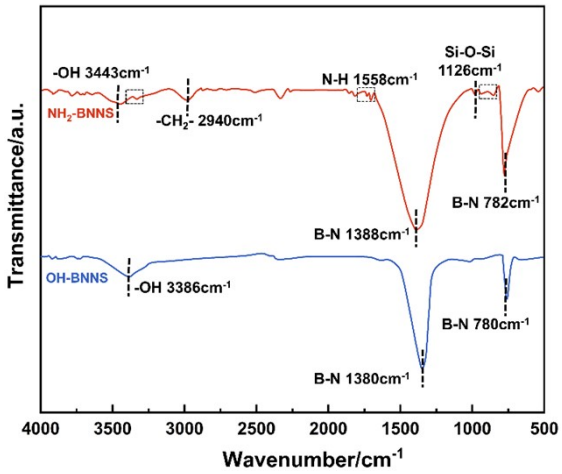

Fig. S4 FT-IR spectra of OH-BNNS and NH_2-BNNS

Figure S4 shows the FT-IR spectra of OH-BNNS and NH_2- BNNS. Both of those have characteristic peaks at 780 cm^{-1} and 1380 cm^{-1}, which are attributed to the B-N atomic reticular planar stretching vibration and deformation vibration. Hydroxyl groups, as nucleophiles, easily attach to electrophilic boron sites in BNNS, primarily at the edges. The characteristic peak at 3386 cm^{-1} is the stretching vibration of -OH on the BNNS sheet, which indicates that the hydroxyl group has successfully functionalized BNNS.

In addition, some new absorption peaks appeared in the FT-IR curve of NH_2-BNNS. Specifically: 2940 cm^{-1} is the absorption peak of the stretching vibration of -CH_2- and -CH_3- in the molecular chain; there is still a characteristic peak of -OH at 3443 cm^{-1}, which may be the incompletely reacted B-OH on the surface of BNNS and the Si-OH generated by the hydrolysis of KH550, but the absorption peak at 3330 cm^{-1} shows that it may also be related with the stretching vibration of N-H. Moreover, the absorption peaks at 890-1100 cm^{-1} may be due to the superposition of the vibrational absorption peaks of -Si-O- and -N-B-O- bonds, and the absorption peak at 1126 cm^{-1} is probably attributed to the formation of -Si-O-Si- by the condensation reaction of Si-OH and B-OH. The presence of -Si-O-Si- and -Si-O- bonds confirms the successful grafting of KH550 onto the BNNS, indicating NH_2 functionalized BNNS successfully.

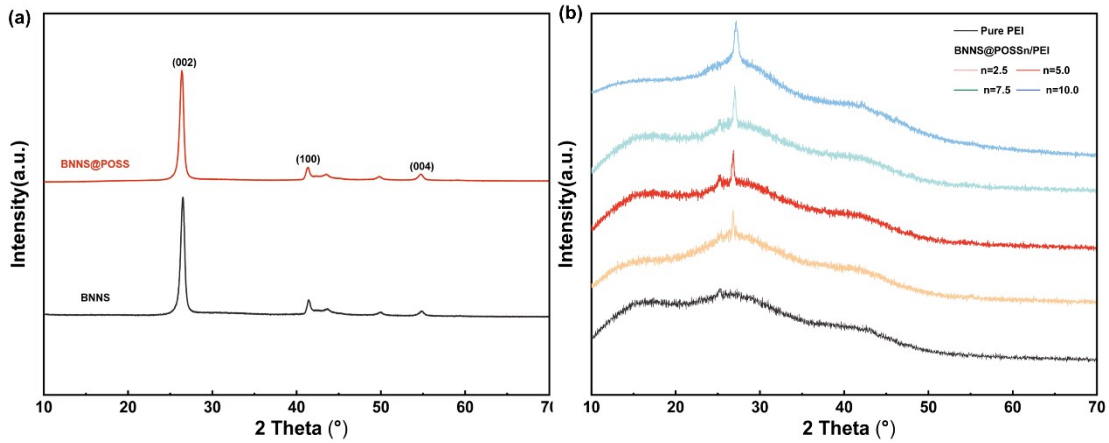

Fig. S5 XRD spectra of BNNS and BNNS@POSS(a), XRD spectra of Pure PEI and BNNS@POSSn/PEI(b)

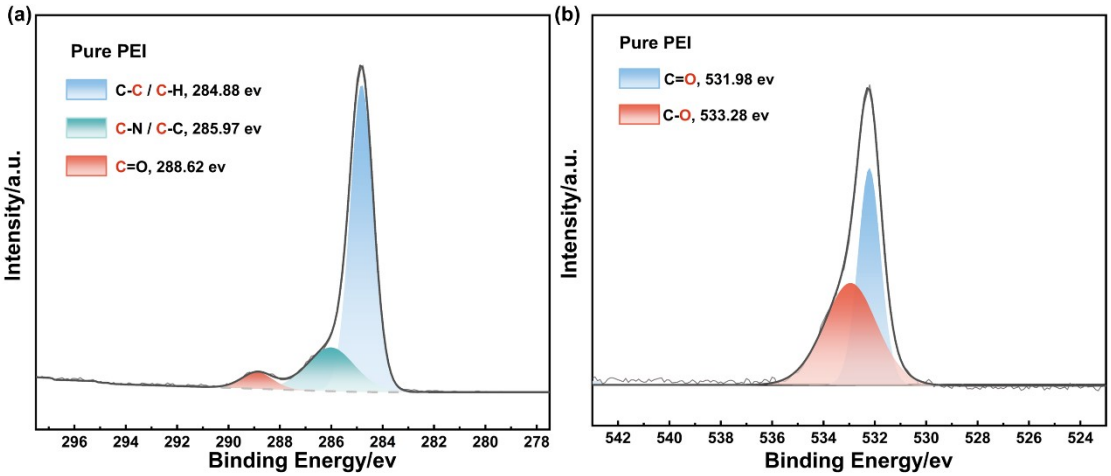

Fig. S6 The C 1s(a) and O 1s(b) spectra of Pure PEI BNNS@$POSS_5$/PEI

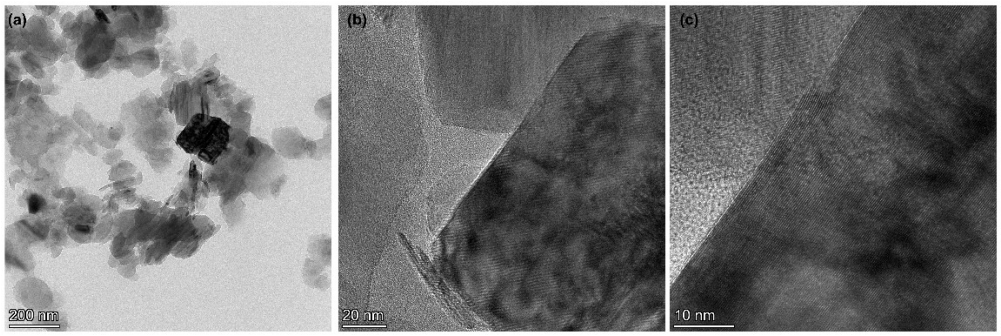

Fig. S7 HRTEM images of NH_2-BNNS

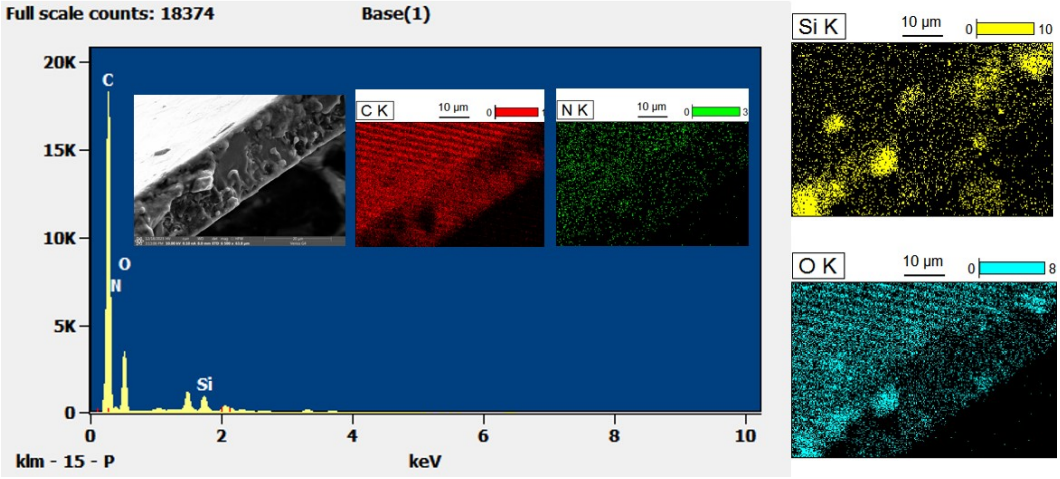

Fig. S8 SEM scan of section after liquid nitrogen quench fracture of BNNS@POSS/PEI at 10 wt% addition amounts

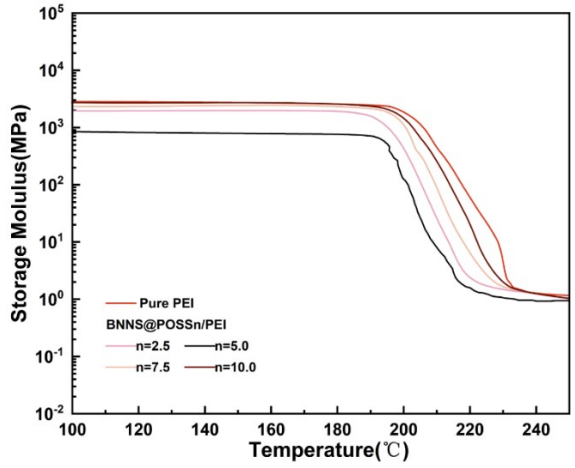

Fig. S9 The storage modulus curves from DMA of Pure PEI and BNNS@POSSn/PEI

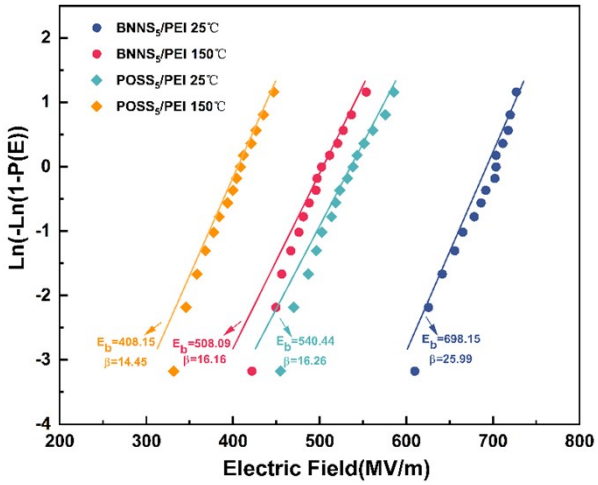

Fig. S10. Weibull statistic of the breakdown strength of $BNNS_5$/PEI and $POSS_5$/PEI at different temperatures

Compared with pure PEI films, the breakdown strength of composite films with 5 wt% of BNNS or POSS was improved. Among them, $BNNS_5$/PEI with a large number of BNNS nanosheets resulted in more complex breakdown paths and higher breakdown strengths at both room temperature and 150 °C. $POSS_5$/PEI showed a slight increase in breakdown strength due to the cage skeleton of POSS, the wide bandgap, and the interconnecting network formed by the copolymerisation of POSS and PEI.

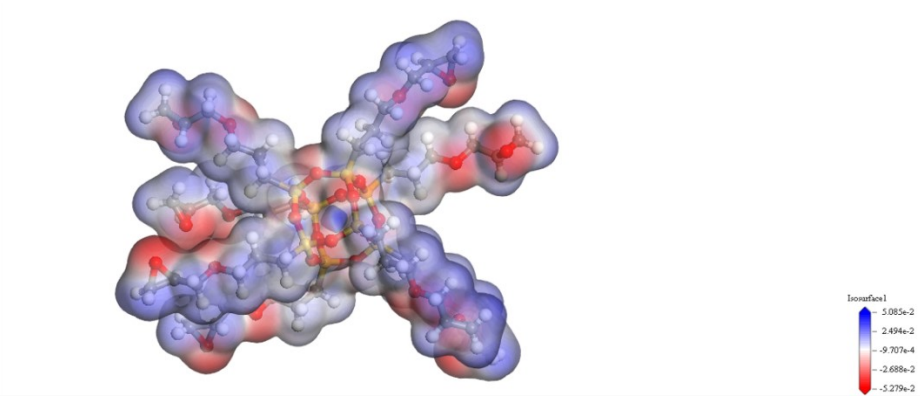

Fig. S11 The electrostatic potential of POSS based on DFT calculations

In the electrostatic potential diagram, the red region with negative electrostatic potential is the electron-rich region. The calculation of POSS reveals that the inside of the cage skeleton of POSS is the blue region where the electrostatic potential is positive, i.e., the electrophilic electron-deficient region, which has a stronger electron-absorbing ability, indicating that the cage cavity structure of POSS is able to be used as a trap to capture free-moving carriers.

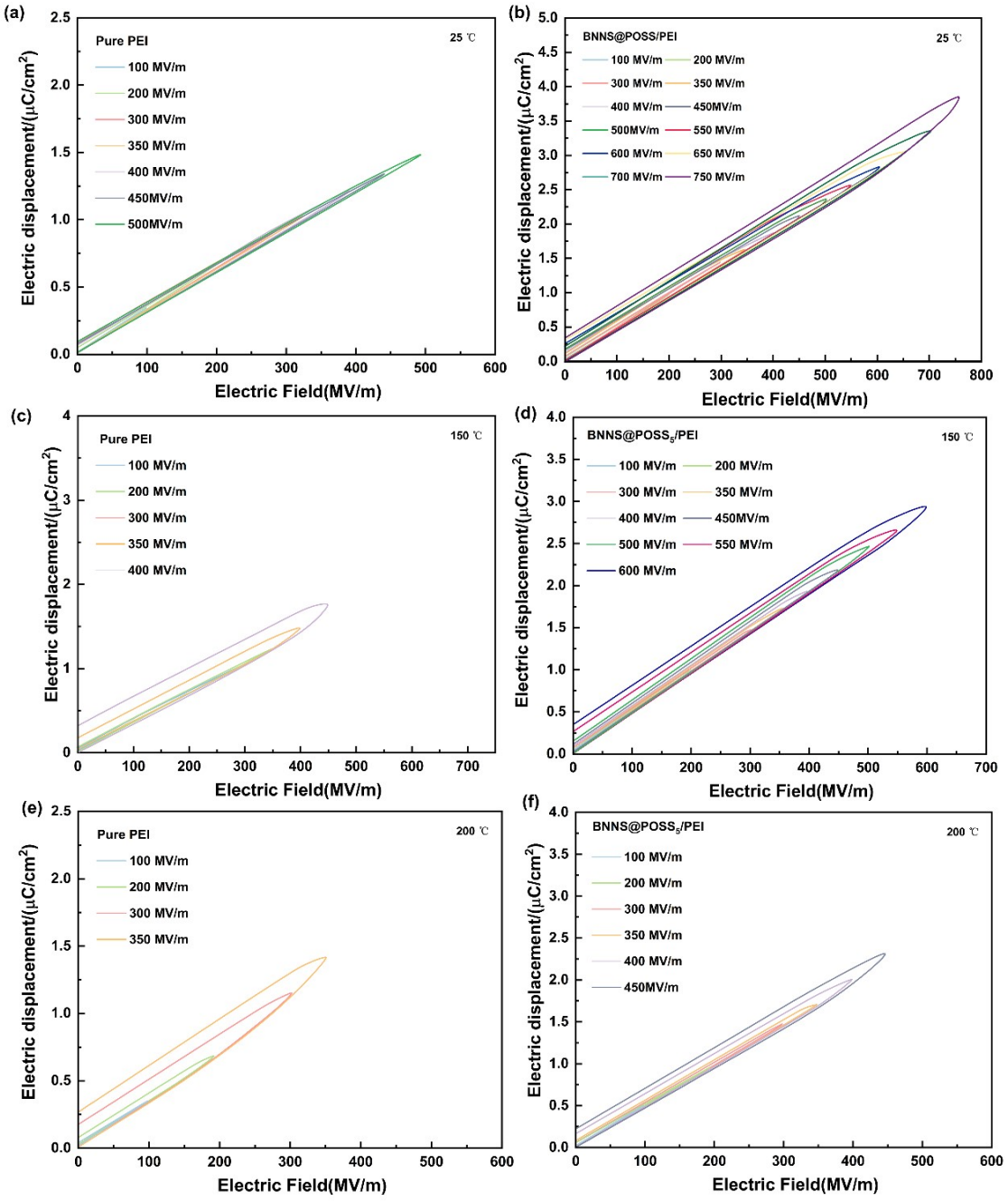

Fig. S12 The D-E loops of Pure PEI and BNNS@POSSn/PEI at 25℃(a-b), 150℃(c-d) and 200℃(e-f).

Table S3. The properties of BNNS@POSS$_5$/PEI and other reported films at 150 ℃

Modified systems	ε_r (at 1MHz)	E_b (MV/m)	U_d (μC/cm²)	η (%)	Ref.
PI(Kapton)	3.35	340	0.82(150°C)	85.0 (150°C)	[13]
PEI(Ultem)	2.8~3.5	460	1.17(150°C)	90.0(150°C)	[1]
BOPP	2.2	580(70°C)	1.80(70°C)	90.0(70°C)	[1]
PEEK	3.00	250	0.49	30.0	[30]
FPE	2.10	350	1.29	19.0	[30]
PEI	3.12	398	1.45	85.6	This work
PEI/Al_2O_3	3.00	525	1.69	93.0	[19]
ZIF-67/PEI	3.43	400	4.59	80.6	[27]
FPE/PDs	3.60	500	3.10	65.0	[6]
ITIC-PI/PEI	3.50	500	4.10	90.0	[12]
PEI-CO-PAA/BNNS	4.20	525	7.40	55.0	[2]
PEI/Al_2O_3@ZrO_2	4.00	525	5.19	93.5	[11]
$BaTiO_3$@TiO_2@SiO_2/PEI	8.40	442	5.41	63.0	[20]
POSS/PI	3.00	610	5.90	81.0	[1]
BNNS/PI	4.15	525	5.30	93.0	[3]
BNNS@AO/PEI	3.80	510	5.90	93.5	[18]
BNNS@POSS/PEI	4.88	614	6.16	90.0	This work

Table S4. The Ud and ηof BNNS@$POSS_5$/PEI and other reported films at 200 °C

Modified systems	categorization	U_d (μC/cm²)	η (%)	Ref.
PI(Kapton)	Commercial Organic Dielectrics	0.12	90.0	[13]
PEI(Ultem)	Commercial Organic Dielectrics	0.80	90.0	[1]
PEI-Al_2O_3	Dielectrics modified with inorganic fillers	2.50	90.0	[19]
PEI/BNNS		2.20	90.0	[30]
H-Al_2O_3/PEI		4.22	90.0	[43]
C-BCB/Al_2O_3		1.48	90.0	[14]
BNNS@POSS/PEI	organic-inorganic hybrid dielectrics	4.12	88.4	This work
PEI/PCBM	Organic semiconductor-modified dielectrics	2.98	90.0	[42]
Al_2O_3/PEI/Al_2O_3	Composite Structured Dielectrics	2.96	90.0	[3]
PEIs/PI/PEIs	Composite Structured Dielectrics	2.08	90.0	[9]